Available online at www.sciencedirect.com
SCIENCE DIRECT
Acta Materialia 54 (2006) 2597–2604
Acta MATERIALIA
www.actamat-journals.com

Phase separation and enhancement of plasticity in Cu–Zr–Al–Y bulk metallic glasses

E.S. Park, D.H. Kim *

Center for Non-crystalline Materials, Department of Metallurgical Engineering, Yonsei University, Seoul 120-749, Republic of Korea

Received 20 September 2005; received in revised form 7 December 2005; accepted 9 December 2005
Available online 24 April 2006

Abstract

Enhancement of plasticity and the occurrence of liquid-state phase separation have been investigated by partially substituting Zr with Y in $Cu_{46}Zr_{47-x}Y_xAl_7$ ($x = 0$, 2, 5, 10, 15, 20, 25, 30, 35) alloys. Since Y has a positive enthalpy of mixing with Zr (+35 kJ/mol) in the liquid state, the alloy composition moves to the metastable miscibility gap of the two amorphous phases with increasing Y content. Phase separation into Y-rich and Zr-rich amorphous phases occurs during cooling from the liquid state when the Y content is above 15 at.%. The bulk amorphous alloys consisting of two phase-separated amorphous phases exhibit extreme brittleness, while the single-phase amorphous alloys containing 2–5 at.% of Y exhibit enhanced plasticity because of the introduction of chemical inhomogeneity in the amorphous matrix. The results indicate that the addition of an element having a positive enthalpy of mixing with the constitutive element in bulk amorphous alloys can increase the plasticity as well as the glass-forming ability, but for a limited composition range.

Keywords: Metallic glasses; Bulk amorphous materials; Positive heat of mixing element; Phase separation; Plasticity

1. Introduction

The discovery of multi-component systems with exceptionally high glass-forming ability (GFA) has made it possible to synthesize bulk metallic glasses (BMGs) of large thicknesses. BMGs have unique mechanical properties, such as high yield strength, high elastic limit, and relatively low Young's modulus [1]. However, one of the major drawbacks of BMGs is their limited global room temperature plasticity. To overcome this limited plasticity, composite microstructures having nano- to micrometer structural inhomogeneities in the amorphous matrix have been designed to enhance the plasticity by multiple nucleation of shear bands and blocking of their propagation [2–5]. Interestingly, however, it has been reported that some monolithic BMGs show enhanced plasticity, although there exists no structural inhomogeneity in the glass matrix. Xing et al. [6], Lee et al. [7], and Park et al. [8] have reported enhanced plastic strain to failure of 4.5%, 6.1%, and 4.2% in as-cast $Zr_{57}Ta_5Cu_{18}Ni_8Al_{10}$, $Ni_{59}Zr_{16}Ti_{13}Si_3Sn_2Nb_7$, and $Cu_{47}Ti_{33}Zr_7Nb_4Ni_8Si_1$ BMGs, respectively. Since these as-cast BMGs exhibit a fully amorphous structure without any evidence of local ordering within the resolution limit of high-resolution transmission electron microscopy (HRTEM), only two possibilities for the enhanced plasticity have been suggested so far: compositional inhomogeneity or structural ordering on the scale of 1–2 nm [6–10]. However, from the alloy chemistry of the BMGs, it is interesting to note that Ta and Nb in the three BMGs mentioned above have a positive heat of mixing with the constituent elements of Zr and Ti (Ta–Zr, Nb–Zr, and Nb–Ti: +13, +17, and +9 kJ/mol, respectively [11]), strongly indicating that compositional inhomogeneity in the as-cast state may be considered as a possible reason for the enhancement of plasticity. In fact, the as-cast BMGs without Ta and Nb exhibit a much lower level of plastic strain, i.e., the plastic strains of as-cast $Zr_{57}Ti_5Cu_{20}Ni_8Al_{10}$, $Ni_{59}Zr_{20}Ti_{16}Si_2Sn_3$, and $Cu_{47}Ti_{33}Zr_{11}Ni_8Si_1$ BMGs are 1.1%, 2.1%, and 1.5%, respectively [6–8]. Recently, Oh et al. reported that a nanoscale phase

* Corresponding author. Tel.: +82 2 2123 4255; fax: +82 2 312 5357.
E-mail address: dohkim@yonsei.ac.kr (D.H. Kim).

1359-6454/$30.00
doi:10.1016/j.actamat.2005.12.020

separation into Cu-enriched and Ag-enriched amorphous phases results in the enhancement of plasticity in $Cu_{43}Zr_{43}Al_7Ag_7$ injection-cast alloy (Cu–Ag: +5 kJ/mol [11]) [12]. Further, it is expected that liquid-state phase separation into two glasses can occur during cooling from the liquid state when the composition is in the range of the metastable miscibility gap for two amorphous phases, as recently observed in $La_{27.5}Zr_{27.5}Al_{25}Cu_{10}Ni_{10}$ (La–Zr: +74 kJ/mol [11]) [13], $Ti_{28}Y_{28}Al_{24}Co_{20}$ (Ti–Y: +58 kJ/mol [11]) [14], and $Ni_{58.5}Nb_{20.25}Y_{21.25}$ (Nb–Y: +127 kJ/mol [11]) [15] alloys.

However, based on the empirical rules for high GFA, it is generally understood that negative heats of mixing among constituent elements are required to obtain an alloy with high GFA. Therefore, addition of alloying elements with positive enthalpy of mixing could reduce the GFA. However, a few papers have reported that the addition of elements with positive heats of mixing promotes GFA [16–20]. It has been shown that the addition of elements with positive heats of mixing can promote the GFA when the element decreases the melting temperature of the alloy: for example, replacement of Zr with Y in $Cu_{46}Zr_{47}Al_7$ alloy (Zr–Y: +35 kJ/mol [11]) [16] and replacement of Cu with Ag and Ni in $Cu_{60}Zr_{30}Ti_{10}$ alloy (Cu–Ag: +5 kJ/mol, Cu–Ni: +26 kJ/mol [11]) [20]. In particular, partial substitution of Zr with Y in $Cu_{46}Zr_{47}Al_7$ alloy significantly improves the GFA, for example enabling the formation of a BMG sample with a diameter of 10 mm from $Cu_{46}Zr_{42}Y_5Al_7$ alloy (3 mm diameter BMG from $Cu_{46}Zr_{47}Al_7$ alloy) by the Cu mold casting method [16].

As mentioned above, the addition of an alloying element having a positive enthalpy of mixing can lead to the improvement of GFA and plasticity, and also can lead to phase separation in the liquid state forming two amorphous phases in the as-cast state. However, in most BMG systems the GFA is reduced significantly with an increasing amount of the element with positive enthalpy of mixing. We note that the Cu–Zr–Al–Y alloy system is a good candidate for investigation since it shows a good GFA and includes an atomic pair of positive enthalpy of mixing as shown in Fig. 1. In Ref. [16], the effect of replacement of Zr with Y in $Cu_{46}Zr_{47}Al_7$ alloys has been studied up to 10 at.%. In the present study, we further increased the amount of Y in $Cu_{46}Zr_{47}Al_7$ alloy up to 35 at.% to investigate the correlation between GFA, chemical inhomogeneity (liquid phase separation), and compressive plasticity.

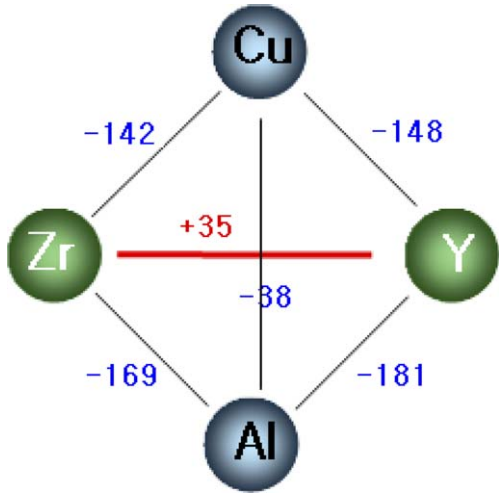

Fig. 1. Relationship of heat of fusion among constituent elements in the Cu–Zr–Y–Al alloy system.

2. Experimental

$Cu_{46}Zr_{47-x}Y_xAl_7$ ($x = 0$, 2, 5, 10, 15, 20, 25, 30, 35) alloy ingots were produced by arc melting high-purity Cu (99.9%), Zr (99.9%), Y (99.9%), and Al (99.9%) under a dynamic Ar atmosphere. Rapidly solidified ribbon specimens were prepared by remelting the alloys in quartz tubes, and injecting them with an over-pressure of 50 kPa through a nozzle onto a Cu wheel rotating with a surface velocity of 40 m/s. The resulting ribbons were about 2 mm wide and 45 μm thick. The injection casting was performed to prepare compression test specimens. Appropriate amounts of the alloys were remelted in quartz tubes and injected through a nozzle into a Cu mold having a cylindrical cavity of 1 mm in diameter.

The structure of the samples was examined preliminarily using X-ray diffraction (XRD; Rigaku CN2301) with monochromatic Cu Kα radiation for a 2θ range of 10–90°. High-resolution neutron diffraction (HRND) experiments were performed using the intense pulsed neutron source of the High-flux Advanced Neutron Application Reactor (HANARO) at the Korea Atomic Energy Research Institute. The HRND data were obtained in a 2θ range of 0–160° using neutrons of wavelengths $\lambda = 0.1835$ nm by 32 monitors with a scanning speed of 0.014°/s.

Thermal analysis of the ribbon samples was carried out to determine the glass transition temperature T_g and the crystallization onset temperature T_x using differential scanning calorimetry (DSC; Perkin–Elmer DSC7) with a constant heating rate of 0.667 K/s. The microstructures of the ribbon samples were examined using HRTEM (JEOL 4010, 400 kV). The thin foil specimens for HRTEM were prepared by Ar ion milling using a Gatan Model 600 at 2.6 keV and ~5 mA with liquid nitrogen cooling. Extreme care was taken with the HRTEM analysis since Cu–Zr–Y–Al thin foils oxidize readily upon exposure in air atmosphere. Chemical compositions were also analyzed using energy dispersive spectrometry (EDS; Oxford 6498) linked with TEM. Compressive tests were performed at a strain rate of 10^{-4} s^{-1}. Specimens were machined from the injection-cast samples into cylinders of 1 mm in diameter and 2 mm in height. The viscosity of the BMG samples as a function of temperature for the amorphous solid and the supercooled liquid was measured using thermomechanical analysis (Perkin–Elmer TMA-7) in the temperature range 675–825 K at a heating rate of 0.667 K/s.

3. Results

XRD results confirmed a fully amorphous structure of the rapidly solidified $Cu_{46}Zr_{47-x}Y_xAl_7$ ($x = 0$, 2, 5, 10, 15, 20) ribbons. Since XRD is not able to detect the dispersion of nanocrystals in Cu-based amorphous alloys [20–22], HRND was performed, which confirmed the amorphous structure of the rapidly solidified $Cu_{46}Zr_{47-x}Y_xAl_7$ ($x = 0$, 2, 5, 10, 15, 20) ribbons. HRND results showed that with an increase of Y content beyond 20 at.%, i.e., in the rapidly solidified $Cu_{46}Zr_{47-x}Y_xAl_7$ ($x = 25$, 30, 35) ribbons, a small amount of crystalline phase was present in the amorphous phase matrix. Fig. 2(a) and (b) show typical HRND data obtained from the rapidly solidified $Cu_{46}Zr_{47-x}Y_xAl_7$ ribbons with $x = 0$ and 25, respectively, indicating the presence of a small amount of crystalline phase in the alloy with $x = 25$. As the amount of Y increased, the position of the diffuse halo peak moved to lower 2θ values, i.e., 47.6° at $x = 0$ to 45.2° at $x = 25$. It is worth noting that the 2θ range of the diffuse halo peak also widened with increasing Y content, i.e., 39.6–57.4° (17.8°) at $x = 0$° to 34.5–56.8° (22.3°) at $x = 25$.

Fig. 3(a)–(g) show DSC traces obtained from rapidly solidified $Cu_{46}Zr_{47-x}Y_xAl_7$ ($x = 0$, 2, 5, 10, 15, 25, 35) ribbons during heating with a heating rate of 0.667 K/s. Clearly the DSC traces can be classified into two groups based on the temperature range of the exothermic reactions: those showing one exothermic reaction with crystallization onset temperatures (T_x) in the range 767–771 K (referred to as peak II) for alloys with $x = 0$, 2, 5, 10; and those showing two exothermic reactions with onset temperatures in the range 578–606 and 733–748 K (referred to as peak I and peak II, respectively) for alloys with $x = 15$, 25, 35. In the case of the alloy with $x = 5$ (Fig. 3(c)), a decrease of heat capacity is clearly observed in the supercooled liquid region (marked on the DSC trace), which is discussed later. The exothermic and endothermic peaks appearing above 800 K marked by arrows in Fig. 3 are not dealt with in detail in the present study. The ratio of the exothermic heats associated with peak I to those associated with peak II in alloys with $x = 15$, 25, 35 increased with increasing Y content. The glass transition temperature (T_g) decreased from 715 K for the alloy with $x = 0$–679.5 K for the alloy with $x = 5$, widening the supercooled liquid region, then increased to 733.5 K for the alloy with $x = 10$. Interestingly, for the alloy with $x = 15$ the glass transition occurred at 717.5 K after the first crystallization reaction, i.e., a part of the sample was crystallized. For alloys with $x = 25$ and 35, glass transition behavior was not observed.

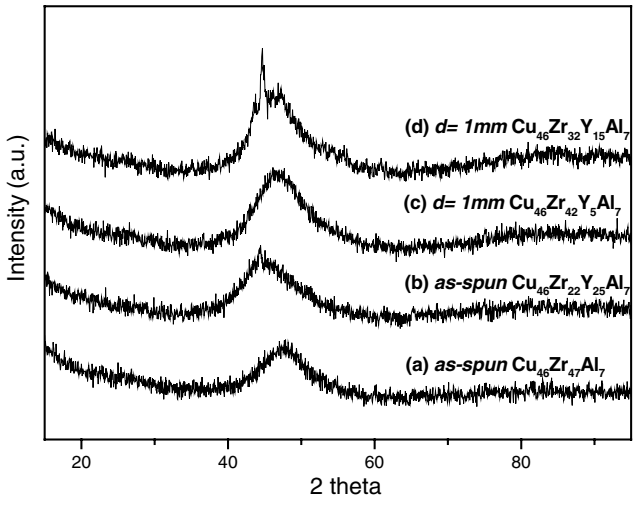

Fig. 2. HRND patterns obtained from $Cu_{46}Zr_{47-x}Y_xAl_7$ alloy samples. As-spun ribbons: (a) $x = 0$, (b) $x = 25$; injection-cast rods (1 mm diameter): (c) $x = 5$, (d) $x = 15$.

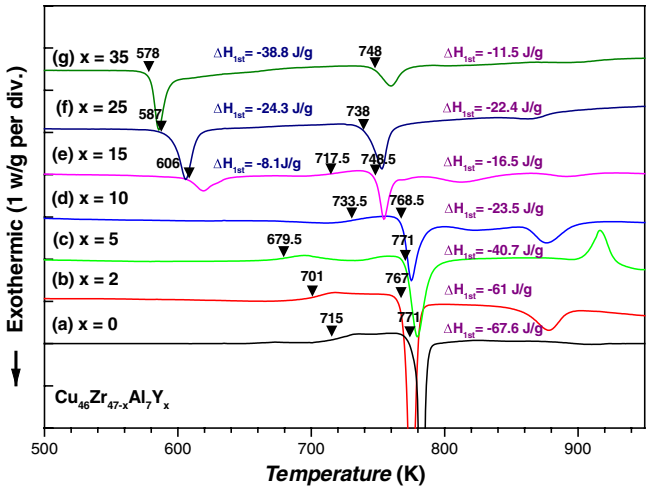

Fig. 3. DSC traces obtained from rapidly solidified $Cu_{46}Zr_{47-x}Y_xAl_7$ ($x = 0$, 2, 5, 10, 15, 25, 35) ribbons.

The HRND (diffuse halo peak widening) and DSC (peaks I and II) results strongly suggest that phase separation into two different amorphous phases might occur in rapidly solidified alloys with Y content above 15 at.%. To confirm the occurrence of phase separation, the as-cast microstructure of the rapidly solidified ribbon with $x = 25$ (this alloy exhibits similar amounts of exothermic heat for peaks I and II: −24.3 and −22.4 J/g, respectively, during crystallization) was observed using TEM. As shown in Fig. 4, the bright-field (BF) TEM image clearly shows the presence of two different amorphous phases with brighter and darker contrasts. From the EDS result the average compositions of the bright- and dark-contrast phases were $Cu_{35.7}Zr_{12.8}Y_{44.3}Al_{7.2}$ (Y-rich) and $Cu_{53.4}Zr_{31.8}Y_{8.3}Al_{6.5}$ (Zr-rich), respectively, confirming that peaks I and II of the DSC trace correspond to crystallization of Y-rich and Zr-rich amorphous phases, respectively. The size scale of Y-rich and Zr-rich amorphous phases is ~50 nm. The characteristic size scale of the inhomogeneity due to primary phase separation has been reported to be very much dependent on the local cooling rate as well as on the alloy system: 25–250 nm in as-melt-spun $Ti_{28}Y_{28}Al_{24}Co_{20}$ ribbon and 0.1–1 μm in as-melt-spun $Ni_{58.5}Nb_{20.25}Y_{21.25}$ ribbon

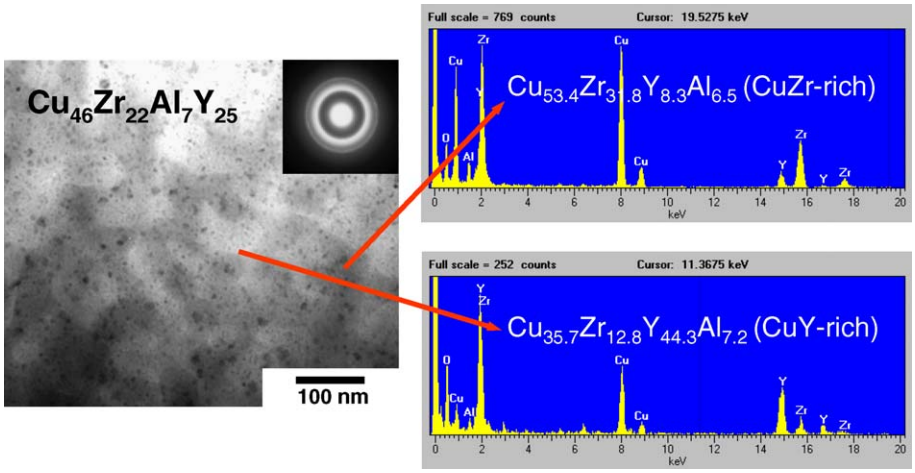

Fig. 4. TEM bright-field image, selected area diffraction pattern (SADP), and EDS results obtained for the as-spun $Cu_{46}Zr_{22}Y_{25}Al_7$ ribbon.

[14,15]. In as-melt-spun $La_{27.5}Zr_{27.5}Al_{25}Cu_{10}Ni_{10}$ ribbon, the upper size limit of the inhomogeneity was about 20 μm [13]. Evidence for secondary phase separation was not observed, possibly due to the smaller temperature range during cooling in the miscibility gap above T_g for the Cu–Zr–Y–Al system. The DSC traces (Fig. 3) indicated that the Y-rich glass did not show glass transition behavior, but the Zr-rich glass showed glass transition behavior (up to 15 at.% Y). The BF TEM image also indicated that partial crystallization occurred due to the deterioration of GFA with increasing Y content, as already shown by the HRND result (Fig. 2(b)). The results indicate that an increase of Y content in the Cu–Zr–Al alloys moves the alloy composition toward the metastable miscibility gap region, thereby forming two different amorphous phases by separation in the liquid state during cooling.

Fig. 5 shows the results of compression tests of injection-cast $Cu_{46}Zr_{47-x}Y_xAl_7$ rods with $x = 0$, 2, 5, 10, 15. To minimize casting defects (oxides, voids, non-melted particles, etc.) [23], the size of the samples used for the tests was 1 mm in diameter and 2 mm in height. The compression test for the alloys with $x = 25$ and 35 could not be performed properly due to extreme brittleness of the bulk

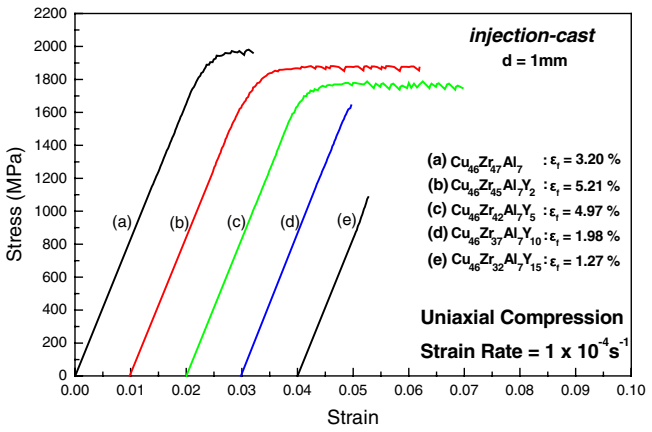

Fig. 5. Stress–strain curves obtained from the uniaxial compression test of $Cu_{46}Zr_{47-x}Y_xAl_7$ ($x = 0$, 2, 5, 10, 15) rod samples of 1 mm in diameter.

samples. The amorphous structure of the rod samples ($x = 0$, 2, 5, 10) for the compression tests was confirmed by XRD and HRND, as shown in Fig. 2(c) for the alloy with $x = 5$. However, the sample with $x = 15$ consisted of a small amount of crystalline phase embedded in the amorphous matrix (Fig. 2(d)). The compression test results (Fig. 5) indicated that the alloys with $x = 0$, 2, 5 exhibited compressive plasticity. In particular, the compressive plastic strain increased with a small increase of Y content (up to 5 at.%), i.e., from 1.2% for $x = 0$–3.3 and 3.1% for $x = 2$ and 5; the compressive fracture strength decreased slightly with an increase of Y content, i.e., 1.96 GPa for $x = 0$ to 1.87 and 1.75 GPa for $x = 2$ and 5. In contrast, the alloys with $x = 10$ and 15 exhibited nearly zero plasticity with compressive fracture strengths of 1.64 and 1.09 GPa, respectively.

Fig. 6 shows scanning electron microscopy (SEM) images revealing the fracture surface and outer appearance of the rod samples ($x = 0$, 5, 10) after the compression tests. The fracture surface for the alloy with $x = 0$ exhibited a vein-like pattern which is attributed to a local change of viscosity along the shear band before fracture of the metallic glass sample. In the case of the alloy with $x = 5$, a locally melted region was observed on the fracture surface (marked in Fig. 6(b)), suggesting that a larger amount of strain along the shear band led to localized melting before fracture. The fractured surface of the alloy with $x = 10$ exhibited a cleavage feature which is characteristic of brittle fracture without forming a shear band. No evidence for a shear band was observed on the outer surface of the sample with $x = 10$, but evidence for multiple shear band formation and propagation was observed clearly on the sample surface of the alloy with $x = 5$.

4. Discussion

The results clearly indicate that the addition of an alloying element having a positive enthalpy of mixing with the constitutive element leads to the improvement of plasticity within a limited composition range (alloys with $x = 2$, 5),

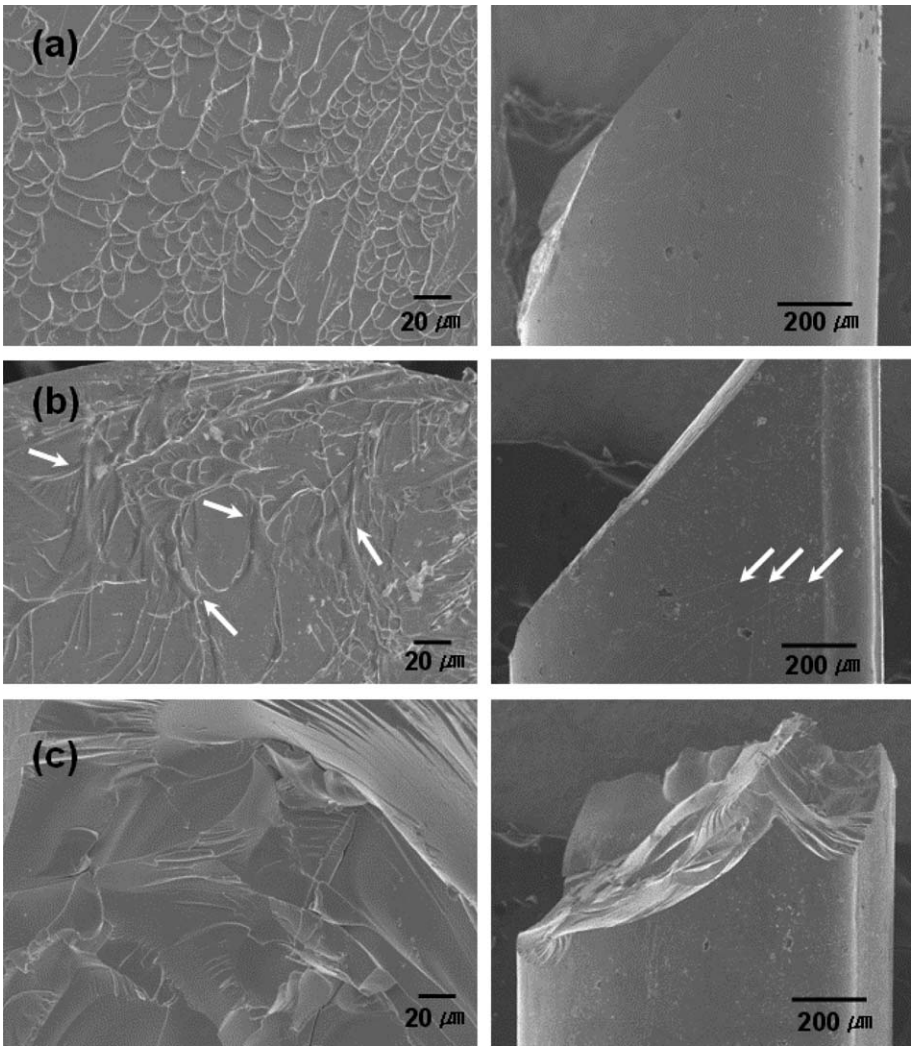

Fig. 6. SEM images revealing the fracture surface and outer appearance of $Cu_{46}Zr_{47-x}Y_xAl_7$ rod samples after compression testing: (a) $x = 0$, (b) $x = 5$, (c) $x = 10$.

although the microstructure is made up of an amorphous structure without any structural ordering within the resolution of HRTEM. Fig. 7(a) shows the HRTEM image and selected area diffraction pattern (SADP) of the as-cast BMG sample with $x = 5$, exhibiting a homogeneous contrast fluctuation and diffuse halo rings, respectively, characteristic of a fully amorphous structure without any evidence for local structural ordering. In contrast, when the alloy composition is such that two-phase glasses are formed by liquid-state phase separation (Y content $\geqslant$15 at.%), the plasticity decreases dramatically, resulting in extreme brittleness. Due to the positive enthalpy of mixing between Y and Zr, phase separation can occur with increasing Y content, strongly indicating that local chemical inhomogeneity can exist even in alloy compositions which solidify into a single amorphous phase from the liquid state. Moreover, the present results indicate that the plasticity can be enhanced by introducing chemical inhomogeneity, but within a limited composition range. The results also indicate that the plasticity can be enhanced when the GFA improves with the addition of an element having a positive enthalpy of mixing with the constitutive element. In $Cu_{46}Zr_{47-x}Y_xAl_7$ alloys, the maximum diameter for glass formation increases from 3 mm for $x = 0$ up to 10 mm for $x = 5$, and then decreases down to 4 mm for $x = 10$ [16]. It is also noted that for previously reported $Mg_{65}Cu_{20}Ag_5Gd_{10}$ [19], $Ni_{61}Zr_{22}Ta_6Nb_7Al_4$ [24], $Ni_{59}Zr_{16}Ti_{13}Si_3Sn_2Nb_7$ [7], $Cu_{43}Zr_{43}Al_7Ag_7$ [25], and $Cu_{47}Ti_{33}Zr_7Nb_4Ni_8Si_1$ BMGs [8], the addition of Ag, Ta, and Nb (Cu–Ag: +5 kJ/mol; Zr–Ta: +14 kJ/mol; Nb–Ta: 0 kJ/mol; Zr–Nb: +17 kJ/mol; Ti–Nb: +9 kJ/mol [11]) simultaneously improves the GFA as well as the plasticity.

The structure of a supercooled liquid can be quantitatively assessed by the fragility index m. The stronger the liquid (higher fragility index) becomes, generally the higher is the GFA. The fragility of the supercooled liquid in the alloys with $x = 0$ and 5 has been measured using the following relationship:

$$m = [D^* T_g^0 T_g]/[\ln 10(T_g - T_g^0)^2], \quad (1)$$

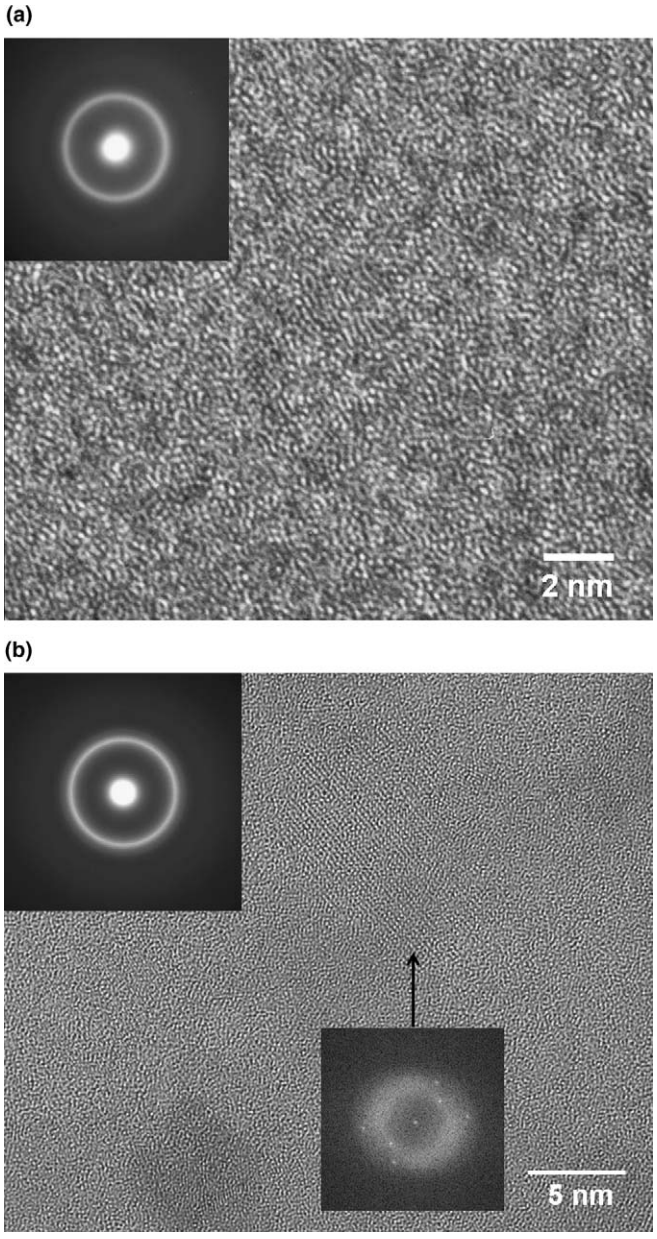

Fig. 7. HRTEM images, SADPs, and diffraction pattern obtained from Fourier transform of HRTEM images for: (a) as-cast BMG rod sample with $x = 5$ (1 mm diameter) and (b) BMG rod sample with $x = 5$ (1 mm diameter) heated to 753 K in the DSC experiment.

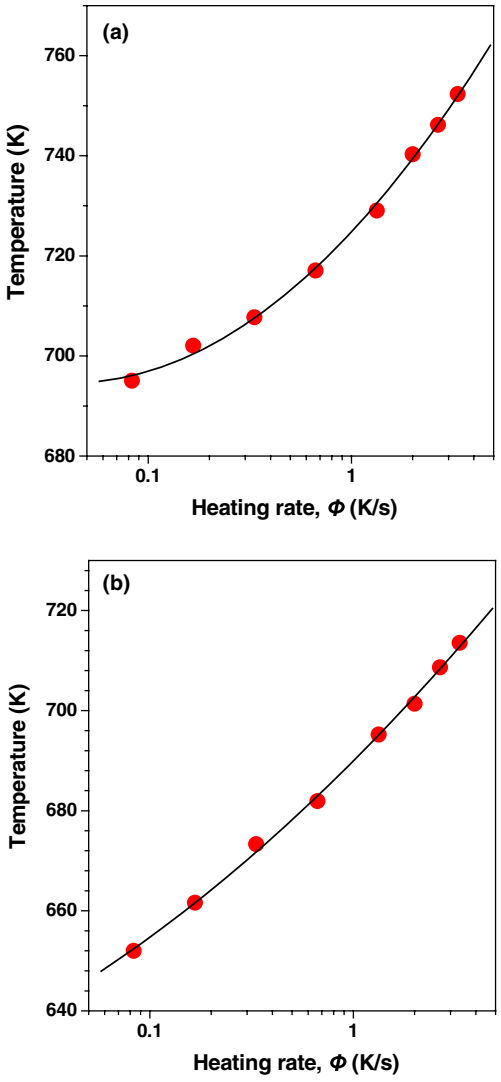

Fig. 8. Onset of the glass transition for: (a) the $Cu_{46}Zr_{47}Al_7$ and (b) the $Cu_{46}Zr_{42}Al_7Y_5$ alloy ribbons as a function of the heating rate Φ.

where $D^*$and T_g^0 are the fitting parameters which can be obtained from the plot of ln Φ (where Φ is the heating rate) vs. T_g. The details of Eq. (1) are described elsewhere [26]. Fig. 8 shows the variation of T_g for the alloys with $x = 0$ and 5 as a function of the heating rate Φ. The best fit to the data yields $D = 0.61$ and $T_g^0 = 640$ for the alloy with $x = 0$ and $D = 3.78$ and $T_g^0 = 502$ for the alloy with $x = 5$. By using Eq. (1), the m values for the alloys with $x = 0$ and 5 evaluated at a heating rate of 5 K/min are 40 and 25, respectively. This shows that in the liquid state the alloy with $x = 5$ is a stronger liquid than the alloy with $x = 0$, i.e., the former has lower energy and higher viscosity in the liquid state, thus exhibiting an improved GFA.

The present study shows that the plasticity and GFA of the BMGs can be enhanced simultaneously when an element with a positive enthalpy of mixing with the constitutive element is included. The substitution of Zr with Y in Cu–Zr–Al alloys can increase the viscosity of the melt due to larger negative enthalpy of mixing of Y–Cu (−148 kJ/mol) and Y–Al (−181 kJ/mol) [11] than Zr–Cu (−142 kJ/mol) and Zr–Al (−169 kJ/mol) [11], improving the GFA. On the other hand, the large difference in enthalpy of mixing of Y–(Cu, Al) (−148 and −181 kJ/mol) and Y–Zr (+35 kJ/mol) [11] can cause a local viscosity inhomogeneity, affecting the formation and propagation of shear bands during compressive plastic deformation. Therefore, the plasticity and GFA can be improved when the addition of the element results in a stronger glass with homogeneously distributed local compositional inhomogeneity. However, the GFA is reduced with a further increase of Y content. Fig. 2(d) shows that partial crystallization occurred during solidification for the $x = 15$ alloy rod (1 mm diameter). With the

formation of nanocrystals (such as shown in Fig. 4), the plasticity is significantly reduced when the Y content is above 10%.

Fig. 9 shows the results of viscosity measurements for the as-cast BMG rod samples with $x = 0$ and 5. The alloy with $x = 5$ exhibited a higher minimum viscosity (η_{min}) of 1.9×10^9 Pa s than the alloy with $x = 0$ (2.8×10^8 Pa s) in the supercooled liquid region, which is consistent with the result of fragility measurements. The viscosity of the alloy with $x = 0$ decreased continuously down to 2.8×10^8 Pa s (~786 K) in the supercooled liquid region, then increased abruptly with the onset of crystallization, as is observed in most of the BMGs. However, the viscosity of the alloy with $x = 5$ started to decrease with increasing temperature, then slightly increased in the supercooled liquid region, showing a local maximum viscosity of 6.0×10^9 Pa s at ~773 K. As marked on the DSC trace for the alloy with $x = 5$ (Fig. 2(c)), it can also be noticed that the heat capacity decreased slightly, and then increased again (i.e., exothermic reaction) in the supercooled liquid region. Increase of viscosity and exothermic reaction in the supercooled liquid region suggests that local chemical inhomogeneity in the as-cast BMG sample with $x = 5$ easily leads to the formation of nanocrystals in the supercooled liquid region during heating for DSC and viscosity measurements.

The HRTEM image, SADP, and Fourier transformed diffraction pattern (Fig. 7(b)) obtained from the BMG rod sample with $x = 5$ heated to 753 K in the DSC experiment clearly shows nanocrystals of ~5–7 nm embedded in the amorphous matrix. The formation of nanocrystals in the supercooled liquid region supports the result that the as-cast BMG rod sample with $x = 5$ exhibits a higher degree of local compositional fluctuation with a small addition of Y than the as-cast BMG rod sample without Y. The local compositional fluctuation in the alloy with $x = 5$ also can be evidenced from the comparison of the effective activation energy for the glass transition (E_g) evaluated using Kissinger's equation [27] for the ribbon samples with $x = 0$ and 5:

$$\ln(T_g^2/\Phi) = \ln(E_g/k_B K_0) + E_g/k_B T_g \quad (2)$$

where k_B is the Boltzmann constant and K_0 is the frequency factor in the Arrhenius law $K_T = K_0 \exp(-E_g/k_B T)$. Fig. 10 shows the linear relationship between $\ln(T_g^2/\Phi)$ and $1/T_g$ for the alloys with $x = 0$ and 5. The values of the activation energy E_g deduced from the slope and intercept have been estimated to be 3.114 and 2.764 eV for the alloys with $x = 0$ and 5, respectively, i.e., the relative stability of glass increased with increasing GFA (with deceasing fragility index). Although the result of the activation energy measurements is not consistent with that expected from the GFA and fragility results, it can be understood by considering that replacement of Zr with Y in Cu–Zr–Al alloys leads to stronger negative bonding between Y and (Cu, Al) as well as positive bonding between Y and Zr. Such a local composition inhomogeneity can result in the lower activation energy for glass transition.

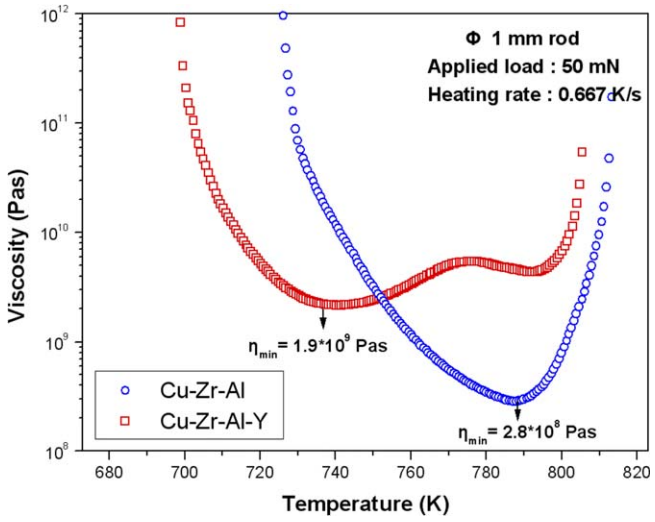

Fig. 9. Result of viscosity measurements for the as-cast BMG rod samples (1 mm diameter): (a) $x = 0$ and (b) $x = 5$.

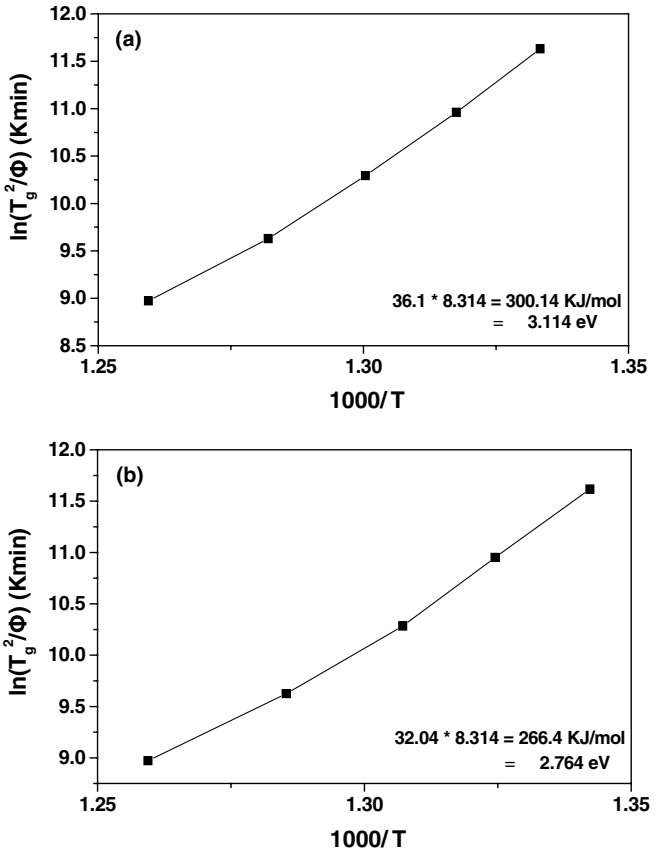

Fig. 10. Relationship between $\ln(T_g^2/\Phi)$ and $1/T_g$ for: (a) the $Cu_{46}Zr_{47}Al_7$ alloy and (b) the $Cu_{46}Zr_{42}Al_7Y_5$ alloy.

5. Conclusions

The present study shows that phase separation in the liquid state occurs when Y, having a positive enthalpy of

mixing with Zr, replaces Zr in Cu–Zr–Al alloys. Phase separation into Y-rich and Zr-rich amorphous phases occurs during cooling when the Y content is above 15 at.% in $Cu_{46}Zr_{47-x}Y_xAl_7$ alloys. The two-phase amorphous alloys exhibit extreme brittleness, while the single-phase amorphous alloys ($x = 2,\ 5$) exhibit enhanced plasticity from the introduction of local chemical inhomogeneity, although the microstructure consisted of an amorphous structure without any structural ordering within the resolution of HRTEM. However, the local compositional fluctuation in the BMG with $x = 5$ can be evidenced from the occurrence of phase separation during solidification with further increasing Y content. A local increase of viscosity and exothermic reaction in the supercooled liquid region supports the conclusion that chemical inhomogeneity in the BMG sample with $x = 5$ leads to the formation of nanocrystals in the supercooled liquid region. The results obtained suggest one effective way of improving the plasticity of BMGs is to add an element (elements) having a positive enthalpy of mixing with the constitutive elements; however, this is only effective for a limited composition range.

Acknowledgements

This work was supported by the Creative Research Initiatives of the Korean Ministry of Science and Technology. The authors acknowledge Dr. B.S. Seong at KAERI for performing the HRND experiment and Ms. H.J. Chang at Yonsei University for performing the HRTEM experiment.

References

[1] Greer AL. Science 1995;267:1947.
[2] Hunfnagel TC, Fan C, Ott RT, Li J, Brennan S. Intermetallics 2002;10:1163.
[3] Ma E. Nat Mater 2003;2:7.
[4] Lee MH, Bae DH, Kim DH, Sordelet DJ. J Mater Res 2003;18:2101.
[5] Wang WH, Dong C, Shek CH. Mater Sci Eng 2004;R44:45.
[6] Xing L-Q, Li Y, Ramesh KT, Li J, Hufnagel TC. Phys Rev B 2001;64:180201(R).
[7] Lee MH, Lee JY, Bae DH, Kim WT, Sordelet DJ, Kim DH. Intermetallics 2004;12:1133.
[8] Park ES, Kim DH, Ohkubo T, Hono K. J Non-Cryst Solids 2005;351:1232.
[9] Fan C, Li C, Inoue A, Haas V. Phys Rev B 2000;61:R3761.
[10] Huang R, Suo Z, Prevost JH, Nix WD. J Mech Phys Solids 2002;50:1011.
[11] Miedema AR, Deboer FR, Boom R. Calphad 1977;1:341.
[12] Oh JC, Ohkubo T, Kim YC, Fleury E, Hono K. Scripta Mater 2005;53:165.
[13] Kündig AA, Ohnuma M, Ping DH, Ohkubo T, Hono K. Acta Mater 2004;52:2441.
[14] Park BJ, Chang HJ, Kim WT, Kim DH. Appl Phys Lett 2004;85:6353.
[15] Mattern N, Kühn U, Gebert A, Gemming T, Zmkerich M, Wendrock H, et al. Scripta Mater 2005;53:271.
[16] Xu D, Duan G, Johnson WL. Phys Rev Lett 2004;92:245504.
[17] Sung DS, Kwon OJ, Fleury E, Kim KB, Lee JC, Kim DH. Met Mater Int 2004;52:1525.
[18] Lee MH, Bae DH, Kim WT, Kim DH. Mater Trans 2003;44:2084.
[19] Park ES, Lee JY, Kim DH. J Mater Res 2005;20:2379.
[20] Park ES, Chang HJ, Kim DH, Ohkubo T, Hono K. Scripta Mater 2006;54:1569.
[21] Jiang JZ, Saida J, Kato H, Ohsuna T, Inoue A. Appl Phys Lett 2003;82:4041.
[22] Park ES, Chang HJ, Kim DH, Kim WT, Kim YC, Kim NJ, et al. Scripta Mater 2004;51:221.
[23] Bei H, Lu ZP, George EP. Phys Rev Lett 2004;93:255506.
[24] Na JH, Park ES, Kim WT, Kim DH, Hono K, unpublished.
[25] Sung DS, Kwon OJ, Fleury E, Kim KB, Lee JC, Kim DH. Met Mater Int 2004;52:1525.
[26] Angell CA. Science 1995;267:1924.
[27] Kissinger HE. J Res Natl Bur Stand A 1956;57:217.